Simulation of flank milling processes

Arnaud Larue, Yusuf Altintas

Simulation of flank milling processes

A. Larue*, Y. Altintas

Manufacturing Automation Laboratory, Department of Mechanical Engineering, The University of British Columbia, 2324 Main Mall, Vancouver, BC, Canada V6T 1Z4

The paper presents prediction of cutting forces when flank milling ruled surfaces with tapered, helical, ball end mills. The geometric model of the workpiece is imported from standard CAD systems, and the tapered helical ball end mill is modeled as the combination of sphere and cone primitives in ACIS© solid modeling environment. The intersection of cutter and part with a ruled surface is evaluated, and the cutter entry into and exit angles from the work material are modeled, and stored as a function of tool center coordinates along the path. The cutter entry and exit angles, the immersion angles, are used as boundary conditions in predicting the cutting forces along the path. The methodology allows prediction of cutting load distribution on the tool and part, as well optimization of machining cycle times by scheduling the feedrate in such a way that torque, power and static deflections can be maintained at safe levels.

Keywords: Flank milling; Feedrate optimization; Various cutter workpiece engagement

1. Introduction

Flank milling operations are common in aerospace industry, especially when milling impellers and blades of the gas turbines. The operations are usually conducted on three-, four- and five-axis machine tools depending on the complexity of the airfoils to be machined. The part is modeled and multi-axis NC tool path is generated in CAD environment. However, the machining process physics is not considered in selecting feeds, speeds and depth of cuts during NC tool path generation step. This paper presents a method which integrates process simulation and optimization to flank milling operations conducted with tapered helical ball end mills.

Majority of the past research in flank milling has been dedicated to modeling of the ruled surface which can be machined in flank milling mode. Wu showed that a blade surface can be flank milled if it can be approximated by a ruled surface [1]. Wu also showed that it is even possible to flank mill more complex surfaces at several passes, as long as each pass can be aligned with a partial rules surface found on the blades. The second challenge is to position the tool in such a way that it does not interfere with the final surface of the blade (Fig. 1a), while keeping the tool trajectory smooth (Fig. 1b) [2]. High speed machining (HSM) requires taking into account of the dynamical properties of recent numerical controller during the tool path generation stage. Chiou et al. presents a swept envelope approach to determine tool position for five-axis machining [3,4]. He presents a closed form solution of the swept profile, and shows 3D shape-generating profiles for generalized cutter shapes [5]. Lartigue et al. [6] developed a method for deforming the top and bottom B-spline curves of the surface in order to minimize the geometric machining errors. Tonshoff et al. [7] and Monies et al. [8] also presented methods to minimize the geometric machining errors, but by manipulating the tool position as opposed to splines of the ruled surface.

Once the tool path generation stage is performed, chatter vibrations and static tool deflections during flank milling process have to be controlled. Indeed, cutting forces vary due to the various engagements of the cutter in the workpiece (Fig. 2), and can lead to geometrical errors on the machined part.

* Corresponding author. Tel.: +1 604 827 5007; fax: +1 604 822 2432
E-mail addresses: larue@mech.ubc.ca (A. Larue), http://www.mech.ubc.ca/~mal (A. Larue).

Nomenclature

r_t	tool radius when the plane of cut related to the top curve of the ruled surface
r_b	radius of the tool's ball nose
γ	half taper angle of the tool
N_r	number of rules on the surface to be machined
N_i	number of planes of cut in z-direction
j	knot number along the ruled surface ($j=0,1,\ldots,N_r-1$)
i	index number of the plane of cut ($i=0,1,\ldots,N_i-1$)
$\vec{n_{Bj}}$	unit normal vector of the machined surface at point B_j
$\vec{n_{Tj}}$	unit normal vector of the machined surface at point T_j
$\vec{k_{Bj}}=v$	unit vector of the rule
$\vec{t_{Bj}}=u$	unit tangent vector of the bottom curve at point B_j representing the machining direction
T_O,u,v,w	local coordinate system
dz	uniform differential height
z_i	height of the ith plane of cut
z_{i+1}	height of the $i+1$th plane of cut
$\vec{k_j}$	unit vector representing the tool axis
$\vec{n_j}$	unit vector perpendicular to the unit tool axis vector and to the unit feed vector at point A_{ij}
$\phi_{s\_calculated}$	effective calculated entry angle
$\phi_{e\_calculated}$	effective calculated exit angle
ϕ_{start}, ϕ_{exit}	entry and exit angles of cut
$Abcurv_x$	curvilinear abscissa in u-direction (machining direction)
pitch_dis	pitch of discretization for immersion angles
N_f	number of flutes
f_z	average feedrate per tooth
p	flute number ($p=0,1,\ldots,N_f-1$)
F_{tp}, F_{rp}, F_{ap}	tangential, radial and axial force acting on pth flute
F_x, F_y, F_z	force components in X, Y and Z direction
dS	differential cutting edge length
db	projected length of an infinitesimal cutting flute in direction along the cutting velocity
dt	differential time interval for digital integration
$d\phi$	differential angular rotation for digital integration
dr	differential radius for digital integration
κ, κ_p	angle between cutting edge normal and Z-axis
K_{tc}, K_{rc}, K_{ac}	cutting force coefficients in tangential, radial and axial directions
K_{te}, K_{re}, K_{ae}	edge force coefficients in tangential, radial and axial directions
Ω	angular velocity of the spindle ($\Omega=2\pi n/60$), n being the spindle speed in rpm
ϕ_p	rotation angle of cutting edge p
$r(z)$, r_i	radius of the cutter at z level (ith plane of cut)
ϕ	total angular rotation for cutting edge on the XY plane
$z_{start}(\phi)$, $z_{exit}(\phi)$	axial integration limits

There has been very little research reported in predicting the cutting forces during flank milling. The cutting force prediction allows identification of loads on the blades during machining, process planning of the machining process to avoid excessive loading of the spindle drive, and it is used as a basis to avoid chatter vibrations [9]. Ramaraj presented the geometry of the tapered helical ball end mill which can be used in predicting the chip load distribution; hence the cutting forces [10]. Altintas et al. [11,12] presented generalized mathematical models which lead to the prediction of cutting forces for any end mill, including tapered helical ball end mills used in flank milling of blades. However, the papers show prediction of cutting forces when the immersion angles are known and the process is stationary. Budak presented process simulation and adaptive machining of impeller as a whole, while considering the force and chatter constraints [13]. He measured the cutting forces, linearized them, and scheduled feedrates along the tool path in order to maintain the load on the cutter and blade at the desired level.

This article presents an alternative to on-line process optimization. It is proposed that the machining forces can be

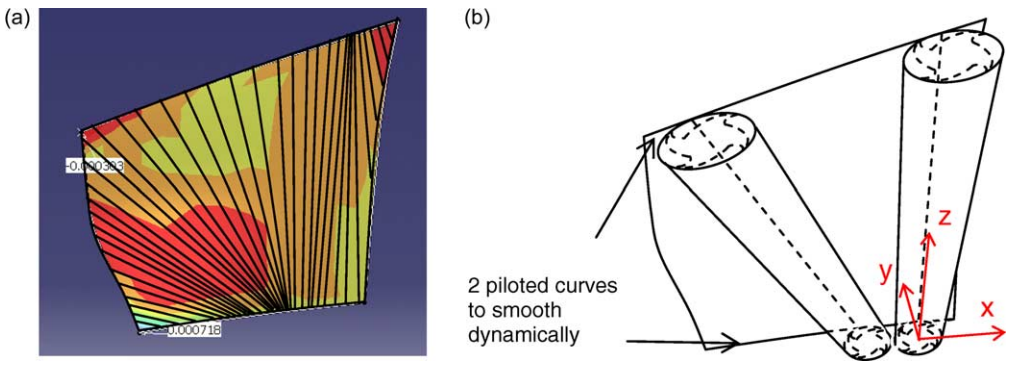

Fig. 1. Tool path generation for five-axis flank milling of impellers.

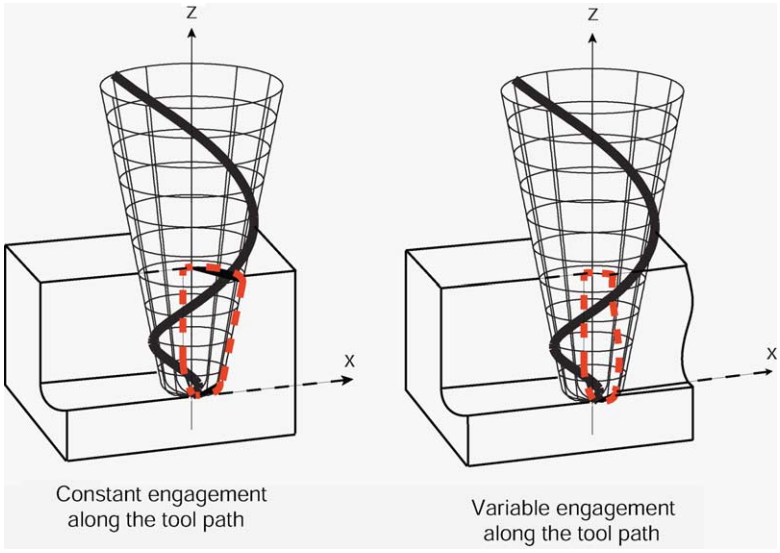

Fig. 2. Variable cutter/workpiece engagement.

predicted in virtual environment by modeling the cutter/part intersection along the tool path, and the feed can be scheduled.

Henceforth, the paper is organized as follows. The tool position is analytically modeled, and an algorithm to evaluate immersion angles from cutter/part intersection is presented in Section 2. The part and tool path are brought from CAD system, and the intersections are evaluated in ACIS© solid modeling environment [14]. The prediction of cutting forces are presented in Section 3, followed by experimental verification of flank milling of sample ruled surface in Section 4. The paper is concluded in Section 5.

2. Prediction of immersion angles

The prediction of cutting forces requires identification of cutter/workpiece intersection boundaries along the tool path when milling ruled surfaces such as flank milling of impellers. The workpiece geometry is assumed to be modeled in a CAD system, and its geometric model is imported using IGES or STEPNC standards. In addition, the NC program can also be imported in the form of industry standard cutter location (CL) file. The flank milling requires orientation of tapered helical ball end mill in such a way that its periphery is tangent to a straight line which connects the upper and lower splines of the ruled surface.

The part is represented by a ruled surface whose parameters are provided in the CAD model. The tapered helical ball end mill is modeled as a combination of a cone and sphere. Both parts are defined in Cartesian coordinate system. Although the concept can be extended to five-axis flank milling of impellers, this paper presents three-axis peripheral milling of a part with ruled outer surface. The immersion history of tapered helical ball end when milling a ruled surface is formulated by modeling tool location, intersection of tool and workpiece with ruled surface, and immersion history along the cutter axis.

2.1. Modeling of cutter location

Consider flank milling of a ruled surface as given in Fig. 3. The top and bottom curves are represented by any parametric spline which is partitioned with equal number of knots. The corresponding knots on the upper and lower curves form straight lines which define the ruled surface with uniform number of patches. The cutter is divided into a number of discrete disc elements along its axis $E_j\vec{C}_{Tj}$ where j represents the knot number along the ruled surface. Each disc is like a circle with varying radius along the tapered helical ball end mill axis. The periphery of the cutter, or each circle along the cutter axis, is tangent to the ruled surface at points B_j and T_j when the tool is cutting the patch j. The cutter's tip is at E_j, the center of the ball end is at C_{Bj}. The cutter body and part are defined using a common coordinate system $O(\vec{X}, \vec{Y}, \vec{Z})$. The rule surface normals at B_j and T_j are given in the CAD model as $\vec{n_{Bj}}$ and $\vec{n_{Tj}}$, respectively. However, they are assumed to be equal here for the simplicity of the immersion calculation. The tool location is defined by the tool tip $E_j(\vec{OE}_j)$ and cutter axis $C_{Bj}\vec{C}_{Tj}$

$$\vec{OE}_j = \vec{OC}_{Bj} - r_b \cdot (1 + \tan(\gamma)) \cdot \frac{C_{Bj}\vec{C}_{Tj}}{\|C_{Bj}\vec{C}_{Tj}\|} \tag{1}$$

where the tool direction is given by $C_{Bj}\vec{C}_{Tj} = \vec{OC}_{Tj} - \vec{OC}_{Bj}$, and position vectors $\vec{OC}_{Bj}$ and $\vec{OC}_{Tj}$ are evaluated from

$$\left.\begin{aligned} \vec{OC}_{Bj} &= \vec{OB}_j + B_j\vec{C}_{Bj} = \vec{OB}_j + \frac{r_b}{\cos(\gamma)} \cdot \vec{n_{Bj}} \\ \vec{OC}_{Tj} &= \vec{OT}_j + T_j\vec{C}_{Tj} = \vec{OT}_j + \frac{r_t}{\cos(\gamma)} \cdot \vec{n_{Bj}} \end{aligned}\right\} \tag{2}$$

where r_b and γ are the ball radius and half cone angle of the tapered ball end mill, see Fig. 3. The vectors $\vec{OB}_j$ and $\vec{OT}_j$ in

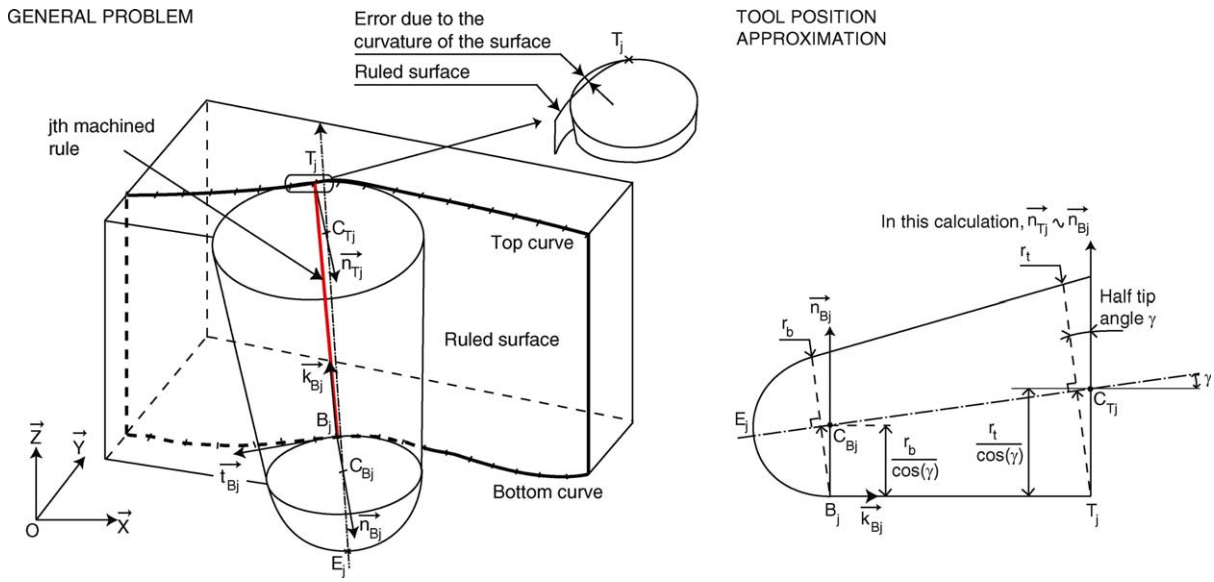

Fig. 3. Tool positioning along a given ruled surface.

Eq. (2) are given in the rule surface model since they are on patch j. The radius of the cutter (r_t) when it is tangent to the surface at point T_j can be expressed from the ruled surface as

$$r_t = r_b + \sin(\gamma) \cdot \|\vec{B_j T_j}\| \tag{3}$$

where $\vec{B_j T_j} = \vec{OT_j} - \vec{OB_j}$. The unit normal ($\vec{n_{Bj}}$) of the ruled surface at B_j is evaluated by the vector products of generated ruled surface contact vector ($\vec{k_{Bj}}$) and the normalized tangent vector ($\vec{t_{Bj}}$) of the bottom curve at B_j

$$\vec{n_{Bj}} = \vec{k_{Bj}} \wedge \vec{t_{Bj}} \rightarrow \vec{k_{Bj}} = \frac{\vec{B_j T_j}}{\|\vec{B_j T_j}\|} \tag{4}$$

Eqs. (1)–(4) define the coordinate and orientation of the tapered helical ball end mill when it is tangent to the ruled surface at point B_j.

2.2. Intersection of tapered helical ball end mill and ruled surface

The intersection of cutter and part along the tool path is evaluated in ACIS© [14] solid modelling environment. Tapered ball end mill is modelled as a Boolean combination of cone and sphere primitives. The surface is imported from the CAD system to ACIS environment by its boundary represented (BREP) model. Since the cutter location and orientation is modelled with respect to the coordinate center in Section 2.1, the engagement of cutter with the workpiece is evaluated using surface/surface intersection operations in ACIS. The ball end and cone primitives are intersected separately with the workpiece for each calculated tool location $\vec{OE_j}$ and $\vec{C_{Bj} C_{Tj}}$ as illustrated in Fig. 4, where the outer surface of the part is a ruled surface while the finish part is a straight plane. Although this example is given here in order to verify the method on the available three and a half axis machining center, the strategy is identical in five-axis milling where each cutter orientation is tangent along a straight line. This example is also practical because it leads to verify the validity of cutting coefficients from various cutter/workpiece engagements while avoiding errors coming from the tool positioning stage. The intersection leads to complete identification of cutter/workpiece engagement boundaries along a given tool path.

For a given tool location, each slice can be intersected with the edges calculated previously. That gives some

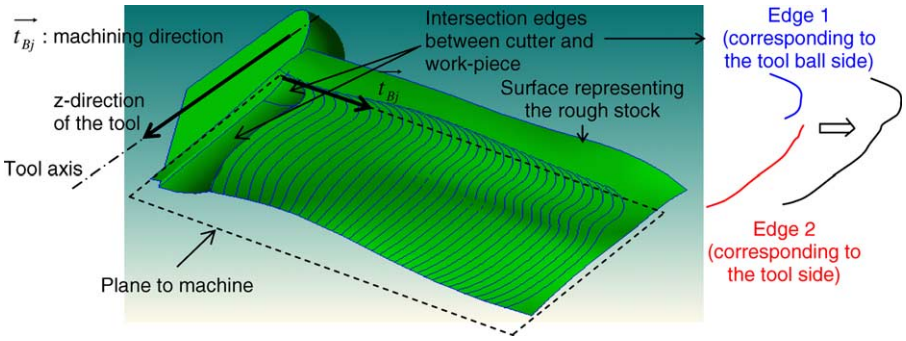

Fig. 4. Intersections between cutter surface and workpiece surface.

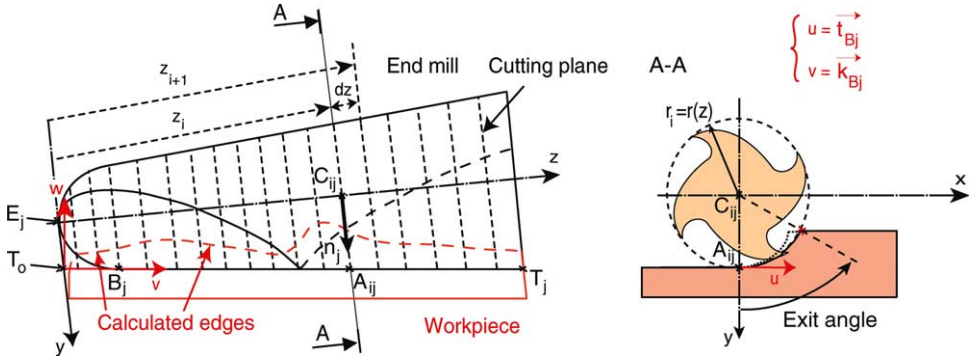

Fig. 5. Cutting planes definition and exit angle calculation.

intersection points. Entry and exit angles can therefore be determined along the z-direction of the tool.

2.3. Evaluation of cutter immersion angles

The aim of the geometric model is to identify cutter entry into and exit from the work material, which is required in predicting the cutting forces in flank milling operations. The tapered cutter is divided into a number of discrete disk elements along its axis, see Fig. 5. Each disk surface is considered as the plane of cut. At the boundary of each disk (i), the cutter cross-section is represented by a circle with varying radius (r_i) along the cutter axis. The immersion at each elevation of the cutter axis, i.e. the entry (ϕ_{start}) and exit (ϕ_{exit}) angles need to be calculated. The cutter may intersect the workpiece with four possible scenarios as shown in Fig. 6.

Case 1. Cutter does not intersect the part.

Case 2. The cutter enters the workpiece with zero entry angle (ϕ_{start}) and exits at (ϕ_{exit}) in up milling, and the reverse is valid for down milling operations. The surface finish point A_{ij} can be calculated by knowing the tool orientation from CL file or as formulated in Section 2.1

$$\vec{OA}_{ij} = \vec{OC}_{ij} + r_i \cdot \vec{n}_j, \leftarrow \vec{n}_j = -\vec{t_{Bj}} \wedge \vec{k}_j \tag{5}$$

where $\vec{t_{Bj}}$ is the unit feed vector along the tool path and $\vec{k}_j$ represents the tool axis, see Figs. 3, 5 and 6. The radius r_i of the cutter disk element at elevation z is given by (Fig. 5):

$$\begin{aligned} r_i &= \|\vec{T_0A}_{ij}\| \cdot \sin(\gamma) + r_b \cdot (1 - \tan(\gamma)) \quad \text{if } \|\vec{T_0A}_{ij}\| \geq r_b \\ r_i &= \sqrt{(r_b^2 - (r_b - (\|\vec{T_0A}_{ij}\| \cdot \cos(\gamma)))^2)} \quad \text{if } \|\vec{T_0A}_{ij}\| < r_b \end{aligned} \tag{6}$$

Case 3. There are two intersection points on either sides of finish surface point A_{ij}. Pt_1 is located on the right-side of A_{ij} which is not in cut and tool starts with zero immersion angle, and Pt_2 is on the left-side of A_{ij} which gives the exit angle of the cut.

Case 4. The cutter starts with nonzero entry angle at Pt_1, and exit at Pt_2.

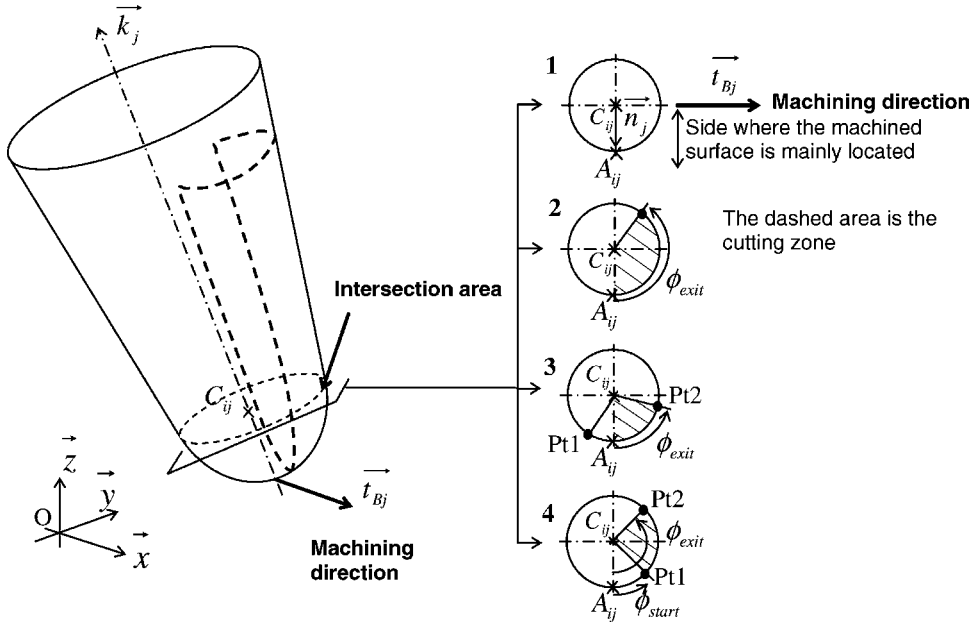

Fig. 6. Particularity of the engagement conditions in flank milling.

Whether the immersion belongs to case 3 or 4 can be identified by evaluating the following vector relationships

$$\left.\begin{aligned}\vec{V}_1 &= \vec{C_{ij}A_{ij}} \wedge \vec{C_{ij}Pt_1}, \quad \vec{V}_1 \cdot \vec{k}_j \\ \vec{V}_2 &= \vec{C_{ij}A_{ij}} \wedge \vec{C_{ij}Pt_2}, \quad \vec{V}_2 \cdot \vec{k}_j\end{aligned}\right\} \tag{7}$$

where $\vec{V}_1$ and $\vec{V}_2$ represent whether the points lie on the left- or right-side of the surface finish point A_{ij}. If $\vec{V}_1 \cdot \vec{k}_j$ has the same sign as $\vec{V}_2 \cdot \vec{k}_j$, the intersection corresponds to case 4, otherwise it is case 3. The surface finish point A_{ij} is calculated by offsetting circle center C_{ij} at amplitude of radius r_i in the direction perpendicular to the feed vector $\vec{t}_{Bj}$. The immersion angles are calculated knowing A_{ij}, C_{ij} and the intersection points Pt_1 and Pt_2.

For example, case 4 leads to verify that $\vec{V}_1$ and $\vec{V}_2$ have the same sign. As a result:

$$\begin{aligned}\phi_{\text{start}} &= \text{angle}(\vec{C_{ij}A_{ij}}, \vec{C_{ij}Pt_1}) \neq 0 \\ \phi_{\text{exit}} &= \text{angle}(\vec{C_{ij}A_{ij}}, \vec{C_{ij}Pt_2}) \neq 0\end{aligned} \tag{8}$$

For case 3, $\vec{V}_1$ and $\vec{V}_2$ have opposite signs. Then, immersion angles are:

$$\begin{aligned}\phi_{\text{start}} &= \text{angle}(\vec{C_{ij}A_{ij}}, \vec{C_{ij}Pt_1}) = 0 \\ \phi_{\text{exit}} &= \text{angle}(\vec{C_{ij}A_{ij}}, \vec{C_{ij}Pt_2}) \neq 0\end{aligned} \tag{9}$$

The direction of spindle rotation, i.e. clock wise (CW) or counter clock wise (CCW), is evaluated according to the logic shown in Fig. 7.

2.4. Interpolation of cutter engagement

A new coordinate system (T_O,u,v,w) has been introduced to display the immersion angles along the considered tool path (Fig. 5). u represents $\vec{t}_{Bj}$, v is $\vec{k}_{Bj}$, where $\vec{t}_{Bj}$ and $\vec{k}_{Bj}$ represent vectors tangent to cutter periphery in radial and axial directions, respectively. T_O is the projection of cutter periphery on y-axis and evaluated as follows:

$$\vec{OT}_o = \vec{OE}_j + r_b \cdot (1 - \tan(\gamma)) \cdot \vec{y}, \leftarrow \vec{y} = \vec{n}_j \tag{10}$$

Therefore along a given tool path, two immersion angles maps representatives of the angular variation of entry and exit angles have been calculated. Fig. 8a illustrates the calculation of intersection points for the previous example. Planes of cut are here represented with circles. Fig. 8b represents the evolution of exit angle along the tool path. In this example, entry angles are always equal to zero.

The immersion angles cards lead to define the most constraint zone on the part to be machined because tool load results from the difference between exit and entry angles. The interpretation of the card can lead either to a re-design of the part or to an optimization of the tool path on critical zones.

Once the immersion angles tables are obtained, the cutting forces simulation can be performed for each tool location. Cutting forces calculation requires to discretize the tool axially and has to be done for every tool locations along the motion according to feedrate requirements.

The cutter/part intersection and the resulting immersion angles are first calculated with large increments in ACIS solid modeling environment, which has high computational cost. As a result, feed per tooth increments are not taken into account.

It is proposed that the immersion angles are calculated at large discrete intervals along the tool path in ACIS, while not causing significant deviations from one station to the next. Then, the resulting immersion angles are interpolated later at finer feed intervals, i.e. feed per tooth increments, using the following proposed method.

The new discretization distance *pitch_dis* has to be calculated. First tool location is assumed to correspond to $u = 0$ and last location to $u = 1$. By calculating the curvilinear abscissa $Abcurv_x$ in u-direction between the first and last tool locations, it is possible to calculate the approximate number of tool rotations necessary to machine the impeller ((floor($Abcurv_x$/$fz \cdot N_f$)). Consequently, we know the interval

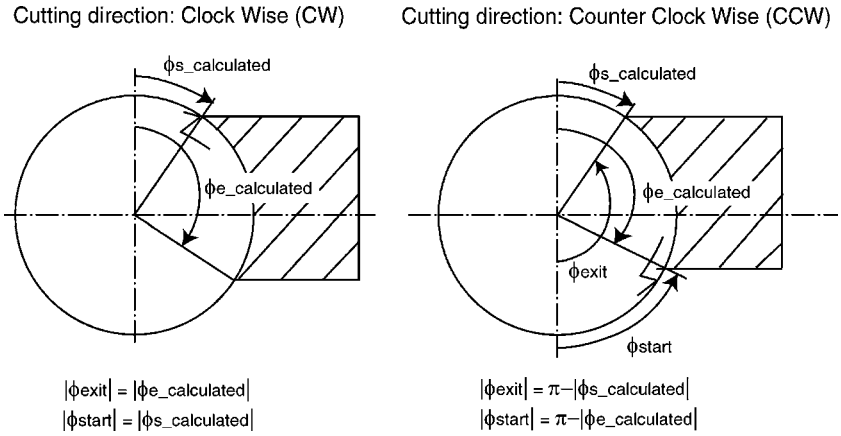

Fig. 7. Taking into account of the direction of the cutting motion.

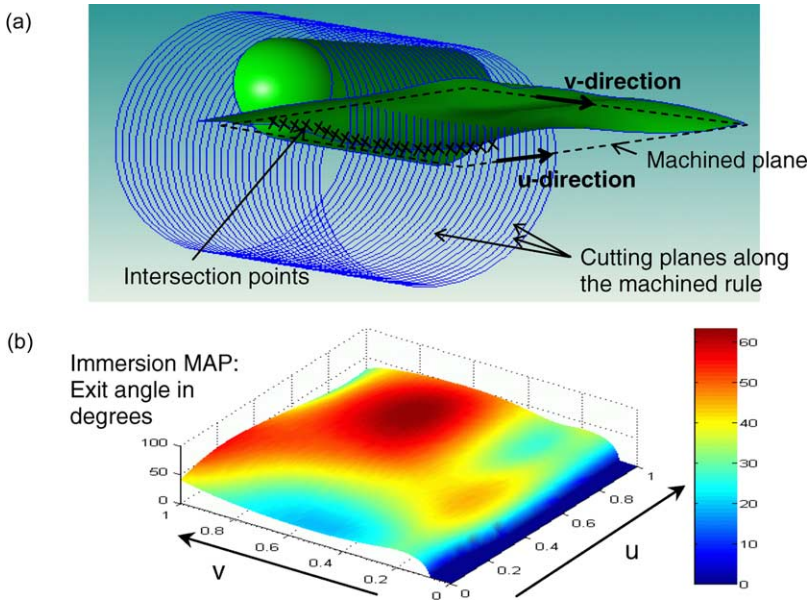

Fig. 8. Various immersion angles calculation.

in u-direction between two tool locations:

$$pitch\_dis = 1/\text{floor}\left(\frac{Abcurv_x}{f_z \cdot N_f}\right) \tag{11}$$

Then, we take advantage of the bi-parametric representation of the immersion map (u,v) by interpolating a new grid of angles considering *pitch_dis*. Interpolation step has been performed in Matlab© software [15] through the use of a function dealing with data interpolation. This function is based on a Delaunay triangulation of the data that uses Qhull method (see http://www.qhull.org/, June 2004).

3. Mechanics of milling with tapered helical ball end mill

The mechanics of tapered helical ball end mill for slot milling operations have been presented before by Engin and Altintas [12], as well as by Ramaraj and Eleftheriou [10] in the past. Hence, only the extension of mechanics in flank milling with varying engagement conditions, and optimization of feedrate to constrain cutting forces will be presented here.

The tapered cutter is divided into a number of discrete disk elements as explained in immersion angle calculation. The model assumes that the $\vec{x}$-axis ($\vec{x} = \vec{t_{Bj}} = u$) is always aligned with the feed direction, the normal to the feed or surface finish is $\vec{y}$ ($\vec{y} = \vec{n}_j$), and the cutter axis is in $\vec{z}$ direction ($\vec{z} = \vec{x} \wedge \vec{y}$). The tool tip is at point E_j, which is used as a reference.

At any cutter disc element, differential cutting forces in tangential (F_{tp}), radial (F_{rp}) and axial (F_{ap}) directions act on each tooth (p) which is within the cut or immersion zone (Fig. 9)

$$\left.\begin{aligned} dF_t &= K_{te}\, dS + K_{tc} f_z \cdot \sin(\phi_p) \cdot \sin(\kappa) db \\ dF_r &= K_{re}\, dS + K_{rc} f_z \cdot \sin(\phi_p) \cdot \sin(\kappa) db \\ dF_a &= K_{ae}\, dS + K_{ac} f_z \cdot \sin(\phi_p) \cdot \sin(\kappa) db \end{aligned}\right\} \tag{12}$$

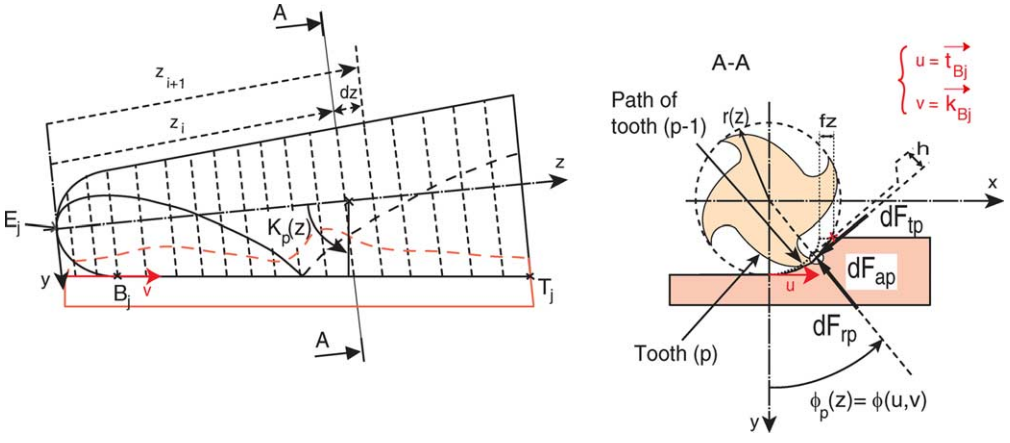

Fig. 9. Cutting forces calculation.

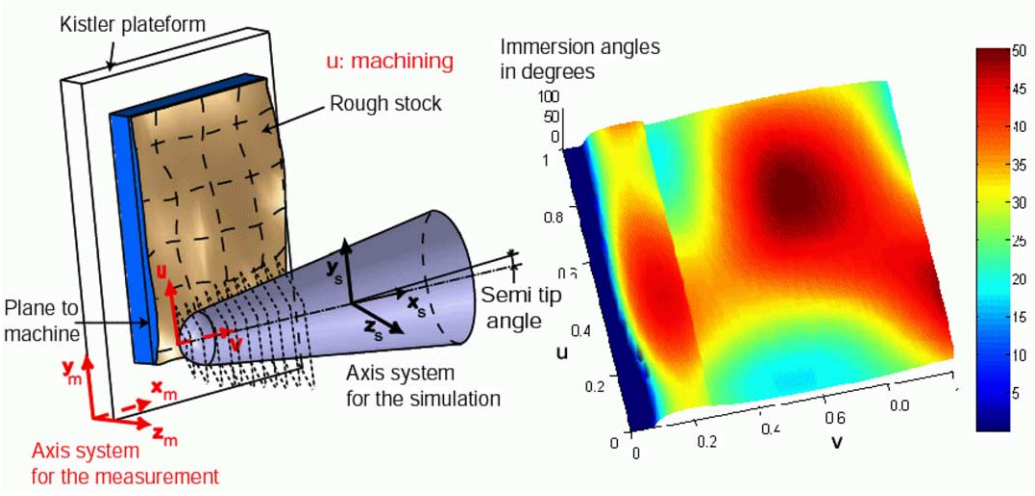

Fig. 10. Cutting forces measurement during the machining.

where f_z is the feed per tooth, $\mathrm{d}b = \mathrm{d}z/\sin\kappa$ and $\mathrm{d}z$ is the axial disk element height, γ is the half taper angle of the cutter, ϕ_p is the instantaneous immersion angle of disk element i which belongs to flute p [16]. The differential cutting edge contact length is $\mathrm{d}S$ and given as $(\mathrm{d}S = |\mathrm{d}r| = \sqrt{r^2(\phi) + (r'(\phi))^2 + (z'(\phi))^2}\cdot \mathrm{d}\phi,\ r'(\phi) = \mathrm{d}r(\phi)/\mathrm{d}\phi,\ z'(\phi) = \mathrm{d}z(\phi)/\mathrm{d}\phi)$ by Engin and Altintas [12]. Note that the flute cuts and produces cutting force only when it is immersion zone, e.g. $\phi_{\mathrm{start}} \le \phi_p \le \phi_{\mathrm{exit}}$. The cutting force coefficients K_{tc}, K_{rc}, K_{ac}, K_{te}, K_{re}, K_{ae} are found either from the material orthogonal cutting data base, or from mechanistic calibration of specific tapered helical end mill as described in [17,18]. The immersion angles may be different at each segment along the cutter axis, but they are calculated in CAD model and stored in an engagement data file which is used as an input by the force prediction and optimization module. The differential forces for each cutter segment along the cutter axis are calculated, projected in three directions $(\vec{x},\vec{y},\vec{z})$,

$$\begin{bmatrix} \mathrm{d}F_{xp} \\ \mathrm{d}F_{yp} \\ \mathrm{d}F_{zp} \end{bmatrix} = \begin{bmatrix} -\sin\phi_p \sin\kappa_p & -\cos\phi_p & -\sin\phi_p \cos\kappa_p \\ -\cos\phi_p \sin\kappa_p & \sin\phi_p & -\cos\phi_p \cos\kappa_p \\ -\cos\kappa_p & 0 & -\sin\kappa_p \end{bmatrix} \times \begin{bmatrix} \mathrm{d}F_{rp} \\ \mathrm{d}F_{tp} \\ \mathrm{d}F_{ap} \end{bmatrix}$$

and summed to find total feed (x), normal (y) and axial (z) cutting forces acting on the cutter

$$\begin{aligned} F_x(\phi) &= \sum_{p=1}^{N_{\mathrm{f}}} F_{xp}[\phi_p(z)] = \sum_{p=1}^{N_{\mathrm{f}}}\sum_{i=1}^{N_i}\int_{z_i}^{z_{i+1}} [\mathrm{d}F_{xp}]\mathrm{d}z \\ F_y(\phi) &= \sum_{p=1}^{N_{\mathrm{f}}} F_{yp}[\phi_p(z)] = \sum_{p=1}^{N_f}\sum_{i=1}^{N_i}\int_{z_i}^{z_{i+1}} [\mathrm{d}F_{yp}]\mathrm{d}z \\ F_z(\phi) &= \sum_{p=1}^{N_{\mathrm{f}}} F_{zp}[\phi_p(z)] = \sum_{p=1}^{N_{\mathrm{f}}}\sum_{i=1}^{N_i}\int_{z_i}^{z_{i+1}} [\mathrm{d}F_{zp}]\mathrm{d}z \end{aligned} \tag{13}$$

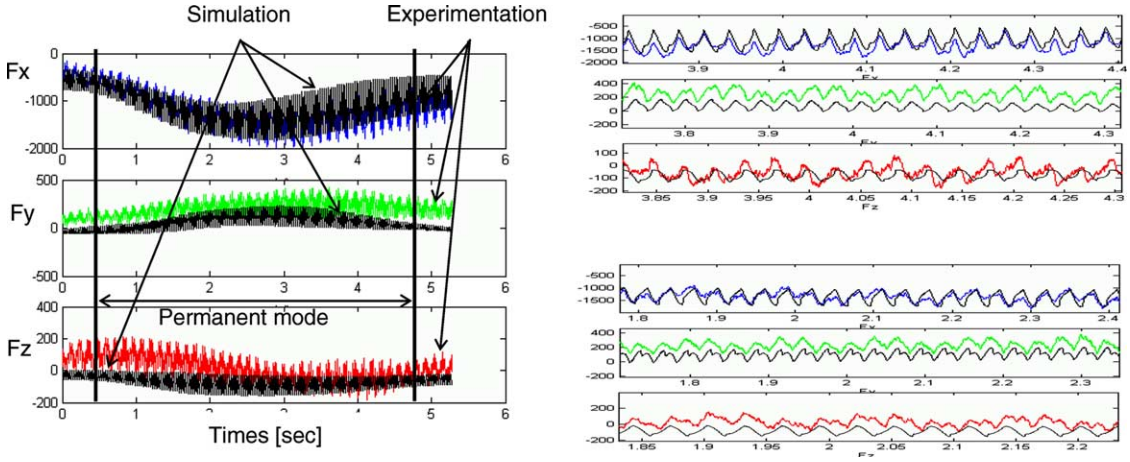

Fig. 11. Comparison between simulated and measured cutting forces.

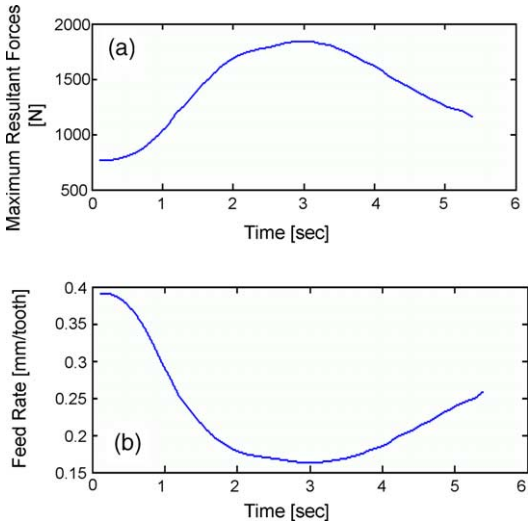

Fig. 12. Feedrate scheduling.

where

- N_f is the number of flutes on the cutter,
- N_i is the number of discrete cutter elements in z-direction,
- z_i and z_{i+1} are the contact boundaries of cutter disk element,
- $\phi_p = \Omega \cdot t$ is the angular position of flute p and disk element i, and Ω is the angular speed of the spindle.

The differential cutting forces are integrated along the full contact length for all flutes which are engaged. For one given angular location $\phi = \Omega \cdot dt$, we obtain $F_x(\phi)$, $F_y(\phi)$ and $F_z(\phi)$ in Cartesian coordinates, where Ω (rad/s) is the spindle speed and dt is the differential time interval for digital integration.

The cutting forces are evaluated at each tool position as a function of material cutting coefficients, feedrate, and local immersion angle at each cutter position and segment and axial immersion depth identified from CAD system. The prediction of cutting forces is used to regulate the feed along the tool path so that the cutter is not overloaded to avoid tool breakage and excessive cutter/impeller blade deflections.

4. Experimental and simulation results

The proposed simulation of flank milling process is experimentally verified on existing three and a half axis horizontal CNC (Mori Seiki HS 402) machining center. As presented in Section 2, the algorithm covers five-axis flank milling process simulation as well, but a five-axis machine was not available in the laboratory for cutting tests. Aluminum AL7075-T6 was prepared with a ruled outer surface as shown in Fig. 10. The cutter was a tapered helical ball end mill with 6.35 mm ball radius, 6.25° half taper angle and four flutes. The cutter/ruled surface intersections are calculated for up milling mode and immersion angles are stored in a file. The identified immersion angle history is shown in Fig. 10.

The first test was conducted at a constant feedrate $f_z = 0.2$ mm/tooth per rev. The spindle speed was

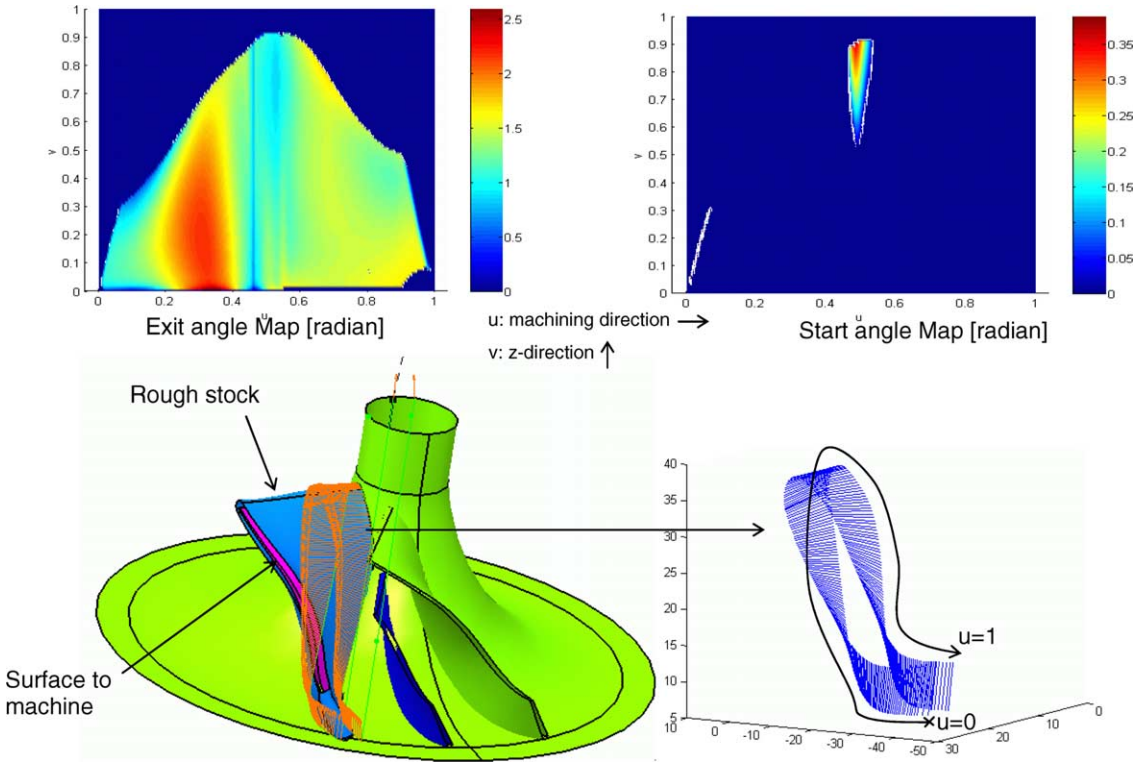

Fig. 13. Immersion cards for the machining of an impeller surface.

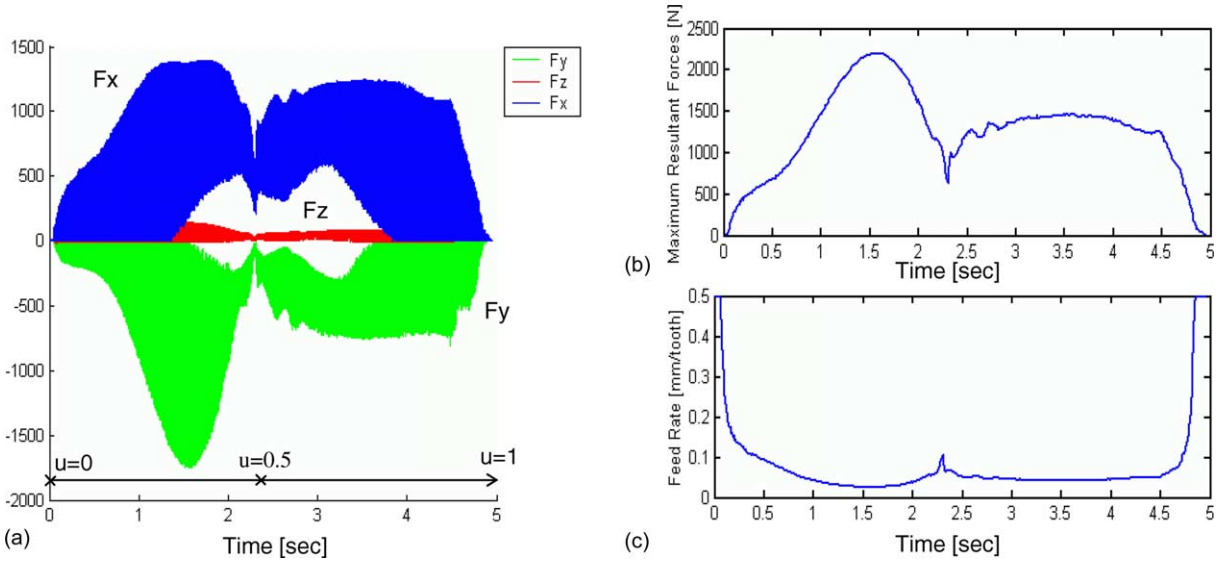

Fig. 14. Virtual scheduling of feedrate during five-axis machining of an impeller surface.

500 rev/min. The simulated and experimental measured cutting force history and a sample close up window of data are shown in Fig. 11. Although prediction accuracy is reasonable, there are some deviations in the normal ($\vec{y}$) and axial ($\vec{z}$) directions which are mainly due to errors in cutting force coefficients and static deflection of the tool in radial direction which changes the effective immersion angle, hence the chip loads.

When the feed is kept constant at $f_z = 0.2$ mm/tooth, the maximum resultant force varies along the tool path as predicted in Fig. 12a. Impellers are usually made from thermally resistant materials such as Titanium and Nickel alloys, and they produce large forces and heat which may break the tool. It is preferred to maintain the cutting force at a safe and desired level so that the cutter is not broken and tool-blade deflections do not violate the tolerance of the part. Using the force prediction algorithm, the feed is scheduled along the tool path so that the resultant force remains at 1500 N regardless of the changes in the cutter engagement conditions along the tool path. The evaluated feedrate history for constant force is given in Fig. 12b.

Although it was not possible to test milling of impeller due to lack of five-axis machining center, Fig. 13 shows a sample simulation. The predicted cutting forces along the finish machining of impeller blade is shown in Fig. 14. The feedrate was 0.1 mm/tooth, and the tool geometry was the same as in previous test. The resultant force is shown in Fig. 14b when the feed is constant at $c = 0.1$ mm/tooth. The feedrate is scheduled to maintain the maximum force, torque and power were constrained at 2500 N, 2000 N mm and 50 kW, respectively. The resulting feed profile is given in Fig. 14c.

5. Conclusion

Simulation model for flank milling processes is presented. The part/cutter intersection boundaries are evaluated using the geometric models of the tapered helical ball end mill and ruled surface to be machined. The cutter immersion angles are extracted from the geometric model, and used as boundary conditions in predicting three to five-axis flank milling operations with tapered helical ball end mills. The cutting forces are predicted, and compared favorably with the measured cutting forces. The model allows scheduling of the feedrate along the complex tool path so that the cutting forces acting on the cutter and blade are kept at the desired but also at productive levels. The model can be used for both three- and five-axis flank milling operations where the final- and semi-finished workpiece geometry is known.

Acknowledgements

This research has been supported by National Science and Research Council of Canada and Pratt & Whitney Canada as part of Virtual Machining Research Chair.

References

[1] C.Y. Wu, Arbitrary surface flank milling of fan, compressor and impeller blades, Transactions of the ASME, Journal of Engineering for Gas Turbines and Power 117 (1995) 534–539.

[2] C.Y. Wu, Y. Altintas, R.A. Thompson, Tool positioning and feedrate problems in impeller flanks milling, Proceedings of the Canadian Conference on Industrial Computer System, McMaster University, Hamilton, Ont., Canada 1982; 13.1–13.6.

[3] J.C.J. Chiou, Accurate tool position for 5-axis rule surface machining by swept envelope approach, Computer Aided Design 36 (10) (2004) 967–974.

[4] J.C.J. Chiou, Y.S. Lee, Swept surface determination for 5-axis numerical control machining, International Journal of Machine Tools and manufacture 42 (2002) 1497–1507.

[5] J.C.J. Chiou, Y.S. Lee, A shape-generating approach for multi-axis machining G-buffer models, Computer Aided Design 31 (1999) 761–776.

[6] C. Lartigue, E. Duc, A. Affouard, Tool path deformation in 5-axis flank milling using envelope surface, Computer Aided Design 35 (4) (2003) 375–382.

[7] H. Tonshoff, Optimal tool positioning for 5-axis milling of arbitrary shaped surfaces, Production Engineering 7 (1) (2000).

[8] F. Monies, J.M. Redonnet, W. Rubio, P. Lagarrigue, Improved positioning of a conical mill for machining ruled surfaces, Journal of Engineering Manufacture 214 (7) (2000) 625–634.

[9] Y. Altintas, Manufacturing Automation, Metal Cutting Mechanics, Machine Tools Vibrations and CNC Design, Cambridge University Press, Cambridge, MA, 2000.

[10] T.C. Ramaraj, E. Eleftheriou, Analysis of the mechanics of machining with tapered end milling cutters, Transactions of ASME 116 (1994) 398–404.

[11] Y. Altintas, P. Lee, A general mechanics and dynamics model for helical end mills, Annals of the CIRP 45 (1) (1996) 59–64.

[12] S. Engin, Y. Altintas, Modeling of general milling operations: Part I. End mills, International Journal of Machine Tools and Manufacture 41 (2001) 2195–2212.

[13] E. Budak, Improvement of productivity and part quality in milling of titanium based impellers by chatter suppression and force control, Annals of the CIRP 49 (1) (2000) 31–36.

[14] 3D ACIS© Modeler, Spatial's prominent 3D modeling development technology, http://www.spatial.com/products/3D/modeling/ (June 2004).

[15] Matlab© software, Mathworks Society, http://www.mathworks.com/ (June 2004).

[16] Y. Altintas, P. Lee, Mechanics and dynamics of ball end milling, Transactions of the ASME, Journal of Manufacturing Science and Engineering 120 (1998) 684–692.

[17] E. Budak, Y. Altintas, E.J.A. Armarego, Prediction of milling force coefficients from orthogonal cutting data, Transactions of ASME 118 (1996) 216–224.

[18] J. Gradisek, M. Kalveram, K. Weinert, Mechanistic identification of specific force coefficients for a general end mill, International Journal of Machine Tools and Manufacture 44 (2004) 401–414.